

****FULL TITLE****
*ASP Conference Series, Vol. **VOLUME**, **YEAR OF PUBLICATION***
****NAMES OF EDITORS****

SUPERSOFT X-RAY LIGHT CURVE OF RS OPH – THE WHITE DWARF MASS IS NOW INCREASING

Mariko Kato,¹ Izumi Hachisu,² Gerardo Juan Manuel Luna³

¹*Keio University, Yokohama 223-8521, Japan*

²*Univ. of Tokyo, Tokyo 153-8902, Japan*

³*University of SaøPaulo, 05508-900 Sao Paulo, Brazil*

Abstract. The recurrent nova RS Ophiuchi, one of the candidates for Type Ia supernova progenitors, underwent the sixth recorded outburst in February 2006. We report a complete light curve of supersoft X-ray that is obtained for the first time. A numerical table of X-ray data is provided. The supersoft X-ray flux emerges about 30 days after the optical peak and continues until about 85 days when the optical flux shows the final decline. Such a long duration of supersoft X-ray phase can be naturally understood by our model in which a significant amount of helium layer piles up beneath the hydrogen burning zone during the outburst, suggesting that the white dwarf mass is effectively growing up. We have estimated the white dwarf mass in RS Oph to be $1.35 \pm 0.01 M_{\odot}$ and its growth rate to be about $(0.5 - 1) \times 10^{-7} M_{\odot} \text{ yr}^{-1}$ in average.

1. Optical and Supersoft X-ray Light Curves of RS Oph

RS Oph is one of the well-observed recurrent novae and is suggested to be a progenitor of Type Ia supernova. It has undergone its sixth recorded outburst on 2006 February 12 (Narumi et al. 2006) and many observational results are reported (see other papers in this proceedings). Its y magnitude light curve has been obtained throughout the outburst (Hachisu et al. 2006) [the numerical table is provided in Hachisu et al. (2008) in this volume], which shows a mid-plateau phase that lasts 45-75 days from the optical peak followed by a quick decrease (Figure 1).

RS Oph has also been observed with X-ray satellites. We analyzed the *Swift* XRT observations available in the HEAS-ARC' database and extracted the count rate in the energy band of 0.3-0.55 keV binned in 2000 s. (see Hachisu et al. 2007, for more details). The supersoft X-ray (SSX) light curve is plotted in Figure 1 (see also Table 1). The light curve rises at about 30 days after the optical peak and shows a long plateau phase that lasts as long as about 50 days corresponding to a long mid-plateau phase of optical light curve.

2. Modelling of SSX Phase

During the nova outburst hydrogen-rich envelope around the white dwarf (WD) expands to a giant size and strong wind mass-loss occurs. In such stages dynamical calculation codes often encounter numerical difficulties, so we cannot

calculate light curves. For example, one must take off the outermost Lagrange mesh points, which prevents us accurately determining the wind mass-loss rate and calculating the resultant evolution speed of novae.

We have calculated light curve models based on the optically thick wind theory (Kato & Hachisu 1994), which is a quasi-evolution Euler code in which the wind mass-loss rate is accurately obtained as an eigenvalue of a boundary value problem. The photospheric temperature and luminosity are also accurately calculated. Therefore, up to now, the optically thick wind is only the method that can follow the theoretical light curves of novae.

To explain the SSX phase and the optical light curves of RS Oph, we have included effects of heat exchange between the hydrogen-rich envelope and a helium layer underneath. Hydrogen burning produces hot helium ash which accumulates underneath the burning zone because convection may descend quickly after the optical peak. This helium layer grows in mass with time and behave as a heat reserver. In the later phase of the outburst heat flows upward from the hot helium layer, which keeps hydrogen-rich envelope hot enough to emit SSX in a long time. After calculating many models for two parameters, i.e., the WD mass and the hydrogen content of the envelope, we obtain a best fit model as shown in Fig 1a (see Hachisu et al. 2007, for details). This model reproduces the optical light curve and explains reasonably well the X-ray count rate.

Figure 1b and Table 2 show that the wind mass-loss stops when the SSX count rate increases. The total luminosity L is almost constant until day 80 when nuclear burning extinguishes and helium ash layer becomes too cool to provide heat any more. In this way the duration of the SSX phase can be explained only if we assume hot helium ash underneath the hydrogen layer. This helium layer accumulates on the WD although some part of the hydrogen-rich matter is blown off by the wind. Therefore, we conclude that the WD mass is growing though the 2006 outburst.

3. Summary

We summarize our results as follows;

1. The WD mass is estimated to be $1.35 \pm 0.01 M_{\odot}$ from the optical and X-ray light curve fittings.
2. The accreted matter during 21 years before the outburst is estimated from the envelope mass at the optical peak to be $4 \times 10^{-6} M_{\odot}$, 50 – 70% of which is ejected by the wind and the rest 30 – 50% accumulates on the WD. Therefore the net growth rate of the WD is $(0.5 - 1) \times 10^{-7} M_{\odot} \text{yr}^{-1}$.
3. The durations of the mid-plateau phase of optical and the peak plateau phase of SSX suggest the presence of a helium layer which accumulates on the WD. Therefore, the WD mass of RS Oph is now growing.
4. The hydrogen content is expected to decrease by $\Delta X = 0.2 - 0.4$ during the outburst, because convection may quickly descend and unable to mix the helium ash into hydrogen-rich material.

References

Hachisu, I. et al. 2006, ApJ, 651, L141

Table 1. Supersoft X-ray count rates

Time	Count	Time	Count	Time	Count	Time	Count	Time	Count	Time	Count
[day]	[s ⁻¹]	[day]	[s ⁻¹]	[day]	[s ⁻¹]	[day]	[s ⁻¹]	[day]	[s ⁻¹]	[day]	[s ⁻¹]
3.53	-0.20	36.74	1.64	40.52	1.56	47.09	2.07	52.67	2.10	64.59	2.00
11.33	-0.69	36.77	1.59	40.54	1.47	47.16	2.10	52.74	2.08	66.12	2.00
11.40	-0.95	36.79	1.54	40.59	1.52	47.37	2.12	52.81	2.06	66.19	2.00
11.47	-0.78	36.81	1.47	40.61	1.53	47.42	2.08	52.86	2.09	66.26	1.98
13.94	-0.93	36.84	1.50	40.68	1.72	47.44	2.14	52.93	1.99	67.12	1.99
15.96	-0.86	36.86	1.49	41.07	1.12	47.49	2.10	52.97	2.09	67.14	1.99
18.53	-1.02	36.91	1.43	41.12	1.62	47.51	2.12	52.99	2.11	67.18	1.99
18.57	-0.80	36.93	1.46	41.14	1.70	47.83	2.10	53.04	2.11	67.21	1.95
26.33	-0.51	36.98	1.22	41.19	1.74	47.90	2.12	53.06	2.12	67.25	1.99
26.35	-0.51	37.00	1.20	41.21	1.74	48.02	2.09	53.18	2.10	67.28	1.94
29.34	1.07	37.05	1.11	41.26	2.00	48.04	2.09	53.20	2.11	67.32	1.97
29.36	1.06	37.12	1.37	41.28	2.02	48.09	2.09	53.25	2.09	67.35	1.86
30.22	0.48	37.14	1.39	41.33	2.04	48.11	2.12	53.27	2.09	67.51	2.02
30.24	0.59	37.18	1.39	41.35	2.04	48.16	2.08	53.32	2.12	67.53	2.02
32.35	1.21	37.21	1.41	41.40	2.04	48.18	2.13	53.34	2.14	68.67	1.99
32.37	1.19	37.25	1.58	41.42	2.07	48.23	2.14	53.39	1.79	68.74	1.96
33.16	1.78	37.32	1.52	41.47	1.97	48.30	2.12	53.41	1.80	69.66	1.96
33.25	1.86	37.39	1.64	42.46	2.09	48.37	2.11	53.46	2.10	69.68	1.96
33.30	1.95	37.42	1.56	42.53	2.03	48.43	2.10	53.48	2.10	69.73	1.97
33.32	1.88	37.46	1.81	43.13	1.90	48.50	2.07	53.53	2.09	69.75	1.95
33.37	1.88	37.49	1.79	43.20	1.87	48.57	2.13	53.55	2.06	70.59	1.95
33.39	1.94	37.53	1.81	43.27	1.98	48.90	2.10	53.60	2.04	70.61	1.97
33.43	1.94	37.60	1.84	43.34	1.97	49.04	2.10	53.62	1.97	70.66	1.96
33.46	1.94	37.67	1.92	43.41	1.92	49.11	2.09	53.67	2.05	70.68	1.96
33.50	1.85	37.74	1.85	43.48	1.78	49.18	2.09	53.69	1.99	72.35	1.90
33.53	1.88	37.79	1.88	43.55	1.94	49.22	2.08	53.74	1.88	72.37	1.87
33.57	1.92	37.81	1.50	43.94	1.69	49.24	2.10	53.78	2.03	72.42	1.89
33.60	1.86	38.13	2.10	44.01	1.91	49.29	2.05	53.80	2.01	72.49	1.88
33.64	1.18	38.32	2.13	44.08	1.91	49.31	2.07	53.85	1.79	73.30	1.91
33.67	0.96	38.34	2.11	44.15	1.81	49.36	2.07	53.87	2.05	73.34	1.89
33.71	0.37	38.39	2.14	44.20	1.67	49.38	2.08	53.92	2.09	73.37	1.87
33.74	0.34	38.41	2.11	44.22	1.76	49.43	2.06	53.94	2.03	73.41	1.79
33.78	0.27	38.46	2.10	44.27	1.91	49.45	2.04	53.99	2.10	73.43	1.86
33.90	1.34	38.48	2.07	44.29	1.90	49.50	2.06	54.01	2.11	74.22	1.82
33.97	1.66	38.53	1.97	44.34	1.43	49.52	2.06	54.06	2.08	74.29	1.79
34.04	1.94	38.60	1.92	44.36	1.73	49.82	2.10	54.13	1.91	74.36	1.80
34.11	1.98	38.67	2.02	44.41	1.93	49.85	2.12	54.18	2.08	74.43	1.87
34.18	1.99	38.74	2.05	44.43	1.97	50.03	2.12	54.20	2.12	74.48	1.87
34.20	2.01	38.78	2.02	44.48	1.95	50.05	2.13	54.24	1.78	74.50	1.88
34.24	1.68	38.85	1.54	44.50	1.97	50.10	2.09	54.27	1.78	75.17	1.87
34.27	1.56	38.92	0.84	44.55	1.99	50.17	2.08	54.31	2.09	75.22	1.86
34.31	1.28	38.99	0.92	45.15	1.92	50.24	2.07	54.34	2.10	75.24	1.85
34.34	1.45	39.06	1.33	45.17	1.90	50.31	2.04	54.41	2.10	77.23	1.81
34.36	1.57	39.13	1.70	45.22	2.09	50.38	2.09	54.45	2.11	77.25	1.79
34.38	1.69	39.34	1.55	45.29	2.11	50.52	2.16	54.48	2.12	77.30	1.81
34.43	1.90	39.41	1.01	45.36	1.98	51.51	2.12	57.60	2.03	77.37	1.81
34.45	1.95	39.48	0.88	45.43	2.12	51.54	2.11	57.62	2.05	79.15	1.74
34.50	2.07	39.52	1.19	45.47	1.90	51.84	2.14	58.62	2.03	79.18	1.74
34.52	2.04	39.55	1.20	45.49	1.85	51.91	2.11	58.64	1.99	80.52	1.67
35.05	1.86	39.59	1.24	45.56	2.14	51.93	2.12	59.15	2.11	80.56	1.68
36.26	1.51	39.62	1.27	45.82	2.09	51.98	2.12	59.87	2.07	80.59	1.68
36.30	1.51	39.66	1.16	45.89	2.00	52.05	2.11	59.89	2.08	80.63	1.67
36.33	1.52	39.68	1.08	46.03	2.09	52.12	2.12	61.63	2.06	80.66	1.68
36.37	1.54	39.75	1.41	46.07	2.02	52.18	2.10	61.70	2.05	85.15	1.36
36.40	1.53	39.82	1.33	46.10	2.02	52.25	2.12	62.16	2.01	85.19	1.35
36.44	1.59	39.85	1.58	46.14	2.09	52.30	2.09	62.18	2.00	85.22	1.35
36.47	1.62	39.87	1.61	46.17	2.09	52.32	2.12	62.23	2.05	87.14	1.17
36.51	1.50	39.99	1.56	46.21	2.08	52.37	2.12	62.25	2.04	87.16	1.18
36.54	1.43	40.05	1.66	46.24	2.08	52.39	2.14	62.58	2.08	87.21	1.17
36.58	1.38	40.12	1.55	46.28	2.08	52.44	2.12	62.65	2.07	87.28	1.17
36.61	1.20	40.19	1.44	46.30	2.09	52.46	2.13	63.18	2.02	87.35	1.15
36.65	1.47	40.26	1.11	46.35	1.97	52.53	2.08	63.25	2.04	91.03	0.70
36.68	1.41	40.33	0.87	46.37	1.97	52.58	2.10	64.18	2.04	91.10	0.74
36.70	1.70	40.40	1.01	46.42	2.09	52.60	2.09	64.24	1.83	93.57	0.43
36.72	1.65	40.47	1.53	46.49	2.06	52.65	2.10	64.52	1.98	93.90	0.36

Hachisu, I. et al. 2007, ApJ, 659, L153

Hachisu, I. et al. 2008, in ASP Conf. Ser. Vol. xx, RS Ophiuchi (2006), ed. N. Evans, M.Bode, & T. O'Brien (San Francisco: ASP), xxx

Kato, M., & Hachisu, I., 1994, ApJ, 437, 802

Narumi, H., Hirosawa, K., Kanai, K., Renz, W., Pereira, A., Nakano, S., Nakamura, Y., & Pojmanski, G. 2006, iaucircular, 8671

Table 2. Evolutional data of the outburst model

Time [day]	$\log T_{\text{ph}}$ [K]	$\log R_{\text{ph}}$ [cm]	\log (mass loss rate) [$M_{\odot} \text{ yr}^{-1}$]	$\log V$ [cm s^{-1}]	$\log L$ [erg s^{-1}]	$\log g$ [cm s^{-2}]
9.8	4.86	11.04	-4.754	7.990	38.38	4.181
22.1	5.09	10.60	-5.287	8.087	38.40	5.060
27.3	5.16	10.46	-5.507	8.096	38.41	5.342
32.6	5.29	10.20	-5.778	7.971	38.42	5.846
34.8	5.37	10.05	-5.952	7.815	38.43	6.151
38.2	5.50	9.79	-6.490	7.405	38.43	6.679
38.9	5.55	9.69	-6.820	7.154	38.44	6.873
39.1	5.56	9.67	-6.921	7.067	38.44	6.918
39.5	5.63	9.53	0.000	0.000	38.44	7.191
40.5	5.82	9.15	0.000	0.000	38.44	7.948
44.9	5.95	8.89	0.000	0.000	38.44	8.471
50.7	6.03	8.73	0.000	0.000	38.43	8.796
60.6	6.10	8.58	0.000	0.000	38.41	9.093
71.7	6.13	8.51	0.000	0.000	38.39	9.239
78.1	6.14	8.44	0.000	0.000	38.30	9.368
80.8	6.13	8.43	0.000	0.000	38.24	9.399
85.0	6.12	8.41	0.000	0.000	38.16	9.425
89.5	6.09	8.40	0.000	0.000	38.02	9.445
94.4	6.04	8.40	0.000	0.000	37.82	9.460
97.5	6.01	8.39	0.000	0.000	37.70	9.466
100.3	5.99	8.39	0.000	0.000	37.58	9.469
116.4	5.85	8.39	0.000	0.000	37.03	9.480

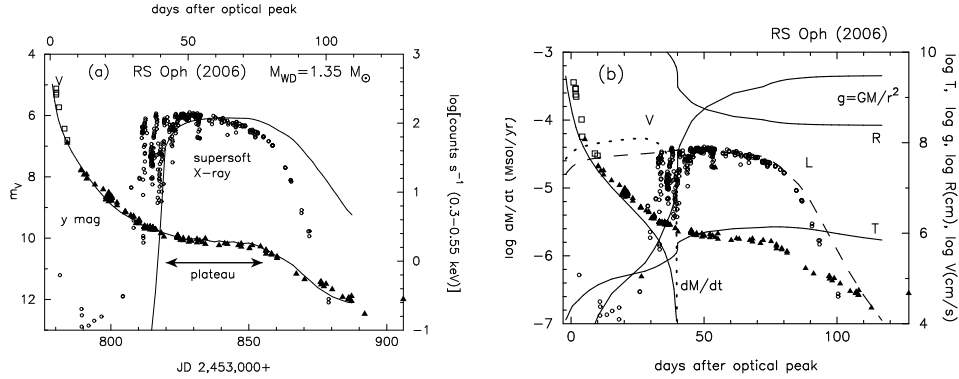


Figure 1. (a) The observational light curves of optical (y band) and supersoft X-ray (0.3-0.55 keV) as well as our best fit model of $1.35M_{\odot}$ WD. (b) The evolution of physical values in our best fit model. The wind mass-loss rate, wind velocity at the photosphere, photospheric temperature, photospheric radius, total luminosity, and the surface gravity $g \equiv GM/r^2$. The scale of the total luminosity $\log L$ is 37.0 (bottom) and 39.25 (top). All the values are plotted in the logarithmic scale. The X-ray count rates and evolution data are tabulated in Tables 1 and 2. The origin of time is set to be JD 2453779.